ARTICLE IN PRESS – Acta Cryst. B

STRUCTURAL SCIENCE
CRYSTAL ENGINEERING
MATERIALS

ISSN 2052-5206

# A temperature-induced order–disorder phase transition in a novel 4-substituted 4,2:6′,4″-terpyridine

## Proof instructions

Proof corrections should be returned by **23 November 2015**. After this period, the Editors reserve the right to publish your article with only the Managing Editor's corrections.

Please
(1) Read these proofs and assess whether any corrections are necessary.
(2) Check that any technical editing queries highlighted in **bold underlined** text have been answered.
(3) Send corrections by e-mail to **jb@iucr.org**. Please describe corrections using plain text, where possible, giving the line numbers indicated in the proof. Please do not make corrections to the pdf file electronically and please do not return the pdf file. If no corrections are required please let us know.

If you wish to make your article **open access** or purchase printed offprints, please complete the attached order form and return it by e-mail as soon as possible.

## Please check the following details for your article

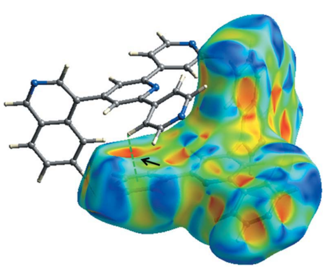

**Thumbnail image for contents page**

**Synopsis:** A temperature driven, single-crystal to single-crystal, first-order phase transition is reported and the structures and interaction schemes in both phases analyzed. A $\pi\cdots\pi \leftrightarrow$ C—H$\cdots\pi$ 'switching' is deemed to be a posible driving force of the transition.

**Abbreviated author list:** Granifo, J.; Westermeyer, M.; Riquelme, M.; Gaviño, R.; Suárez, S.; Halac, E.B.; Baggio, R.

**Keywords:** phase transition; first order; ligand properties; weak interactions; order–disorder



## How to cite your article in press

Your article has not yet been assigned page numbers, but may be cited using the doi:

Granifo, J., Westermeyer, M., Riquelme, M., Gaviño, R., Suárez, S., Halac, E.B. & Baggio, R. (2015). *Acta Cryst*. B**71**, doi:10.1107/S205252061501937X.

You will be sent the full citation when your article is published and also given instructions on how to download an electronic reprint of your article.

STRUCTURAL SCIENCE
CRYSTAL ENGINEERING
MATERIALS

ISSN 2052-5206

Received 21 August 2015
Accepted 13 October 2015

Edited by E. V. Boldyreva, Russian Academy of Sciences, Russia

**Keywords:** phase transition; first order; ligand properties; weak interactions; order–disorder.

**CCDC references**: 1430999; 1431000; 1431001; 1431002; 1431003

**Supporting information**: this article has supporting information at journals.iucr.org/b

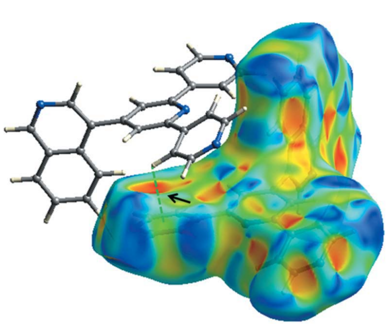



# A temperature-induced order–disorder phase transition in a novel 4-substituted 4,2:6′,4′′-terpyridine

**Juan Granifo,[a]* Marleen Westermeyer,[a] Maricel Riquelme,[a] Rubén Gaviño,[b] Sebastián Suárez,[c,d] Emilia B. Halac[d,e] and Ricardo Baggio[d]***

[a]Departamento de Ciencias Químicas y Recursos Naturales, Facultad de Ingeniería y Ciencias, Universidad de La Frontera, Casilla 54-D, Temuco, Chile, [b]Instituto de Química, Universidad Nacional Autónoma de México, Cd. Universitaria, Circuito Exterior Coyoacán, 04510 México, Mexico, [c]Departamento de Química Inorgánica, Analítica y Química Física, INQUIMAE-CONICET, Facultad de Ciencias Exactas y Naturales, Universidad de Buenos Aires, Buenos Aires, Argentina, [d]Gerencia de Investigación y Aplicaciones, Centro Atómico Constituyentes, Comisión Nacional de Energía Atómica, Buenos Aires, Argentina, and [e]Escuela de Ciencia y Tecnología, Universidad Nacional de San Martín, Provincia de Buenos Aires, Argentina. *Correspondence e-mail: juan.granifo@ufrontera.cl, baggio@cnea.gov.ar

Crystals of 4′-(isoquinolin-4-yl)-4,2′:6′,4′′-terpyridine (*iqtp*), $C_{24}H_{16}N_4$, grown from an ethanol solution, undergo a reversible first-order, single-crystal to single-crystal phase transition at $T_c$ in the range 273–275 K, from a disordered higher-temperature phase [form (I)] in the space group $P2_1/c$, with one single molecule in the asymmetric unit, to an ordered lower-temperature one [form (II)] in the space group $P2_1/n$, with two independent molecules. There is a group–subgroup relationship linking (I)–(II), due to cell doubling and the disappearance of a number of symmetry operations. In addition to X-ray diffraction, the transition has been monitored by Raman spectroscopy and differential scanning calorimetry [disclosing an enthalpy change of 0.72 (6) kJ mol$^{-1}$]. Variations of the unit-cell parameters with temperature between 170 and 293 K are presented. The evolution of diffraction spots in the vicinity of the transition temperature shows the coexistence of both phases, confirming the first-order character of the transition. Structural details of both phases are analyzed and intermolecular interactions compared in order to investigate the mechanism of the phase transition. A three-dimensional Hirshfeld surface analysis was performed to corroborate the significant changes in the intermolecular features.

## 1. Introduction

Even if the studies based on the ligand properties of the 4,2′:6′,4′′-terpyridines, especially those which are 4′-substituted, have grown significantly due to their use as building blocks in coordination chemistry (Housecroft, 2014), the reports have been restricted mainly to coordination polymers (Housecroft, 2014) and molecular metallo-macrocycles (Yoshida *et al.*, 2007; Constable, Housecroft, Prescimone, Vujovic & Zampese, 2014; Constable, Housecroft, Vujovic & Zampese, 2014). Within the set of known 4,2′:6′,4′′-terpyridines functionalized in the 4′-position, the 4-pyridyl substituted 4′-(4-pyridyl)-4,2′:6′,4′′-terpyridine (*ptp*) has proven to be the most versatile. In addition to the above capabilities, it has also been employed as a tridentate ligand in the construction of icosahedral coordination cages (Heine *et al.*, 2011; Constable *et al.*, 2011), by using its divergent N,N′′-atoms and the 4′-pyridyl N atom to link the metal centers. Among the few structural determinations by X-ray diffraction of 4,2′:6′,4′′-terpyridines functionalized in the 4′-position (Constable *et al.*, 2010; Constable, Housecroft, Kopecky, Neuburger, Zampese & Zhang, 2012; Constable, Housecroft, Neuburger, Vujovic, Zampese & Zhang, 2012; Constable, Zhang, Housecroft &

Zampese, 2012*c*; Constable, Housecroft, Neuburger, Schönle, Vujovic & Zampese, 2013; Constable, Housecroft, Schönle, Vujovic & Zampese, 2013; Constable, Housecroft, Vujovic, Zampese, Crochet & Batten, 2013; Constable, Housecroft, Vujovic & Zampese, 2014*b*; Hou & Li, 2005; Klein, Constable, Housecroft, Zampese & Crochet, 2014; Klein, Constable, Housecroft & Zampese, 2014; Singh *et al.*, 2014; Cave & Raston, 2001), only the 4′-(4-(anthracen-9-yl)phenyl)-4,2′:6′,4′′-terpyridine (*aptp*) has a fused-ring system as a substituent. The compound was reported by Constable, Housecroft, Schönle, Vujovic & Zampese (2013), and was unusual owing to the three independent molecules in the asymmetric unit, fundamentally as a result of differences in interplanar angles between aromatic rings. Considering these antecedents we decided to investigate the closely related species 4′-(isoquinolin-4-yl)-4,2′:6′,4′′-terpyridine (*iqtp*), which possesses a similar coordination capacity to *ptp* and where the only difference is the metal-binding fused-ring isoquinolin-4-yl instead of 4′-pyridyl. Unexpectedly, during the structural study by X-ray diffraction we observed a temperature-dependent single-crystal to single-crystal first-order phase transition, a phenomenon that, even if not new in organic crystals (Pal *et al.*, 2014; Drebushchak *et al.*, 2011; Kubicki, 2004), to the best of our knowledge is novel in this type of terpyridine-based compound.

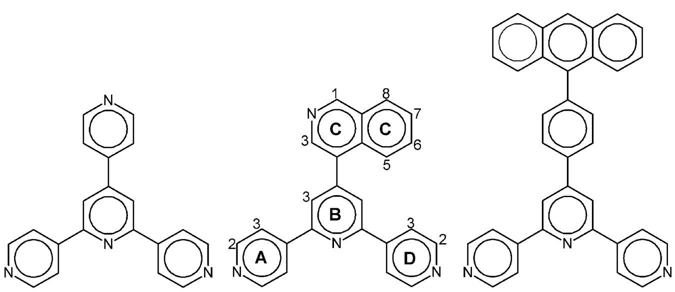

ptp iqtp aptp

Conformational modifications would be expected to exist in molecules like *iqtp* considering that they possess three rotable groups (two pyridyl and one isoquinolinyl) able to adopt multiple torsion angles with respect to the central pyridyl ring mean plane. It is also expected that the presence of only N-containing aromatic groups enables the formation of several specific types of intermolecular contacts (*e.g.* $\pi\cdots\pi$, N$\cdots$H, C—H$\cdots\pi$) and that they should be the key for the stabilization of diverse structural forms. The case reported herein appears as an opportunity to investigate what happens with the interactions between organic molecules when a phase transition takes place, with regard to their balance leading to different structures at both sides of the transition. Thus, in this work a systematic investigation of the temperature-driven phase transition of *iqtp* was carried out. Single-crystal X-ray diffraction (XRD) studies were performed at five different temperatures, well above and below the transition temperature plus two flanking temperatures. Differential scanning calorimetry (DSC) measurements and Raman spectroscopy were also used to monitor the phase transition. Variations of the unit-cell parameters with temperature were also determined. In order to investigate the mechanism of the phase transition the intermolecular interactions at both sides of the transition were compared. A Hirshfeld surface analysis was carried out to visualize the changes in the leading intermolecular interactions. Finally, a few brief considerations are made about the kind of transformation involved, in comparison to those discussed in the vast literature on polymorphism and polymorphic transformations (*viz.* Cruz-Cabeza & Bernstein, 2014; Boldyreva *et al.*, 2015; Bučar *et al.*, 2015 *etc.*).

## 2. Experimental

IR spectra were recorded on an Agilent Cary 630 FT–IR spectrometer with the Varian Resolutions Pro software, using a Diamond ATR (attenuated total reflectance) accessory. An Exeter Analytical CE-440 elemental analyser was used for microanalysis (C, H, N). NMR spectra were recorded on a Bruker Avance 300 MHz. Electrospray ionization (ESI) mass spectra (MS) were measured on a Bruker esquire 6000. Single-crystal X-ray diffraction data were collected using a Gemini diffractometer (Oxford Diffraction). Measurements were performed at different temperatures (170, 220, 274, 277 and 293 K) attained with a Desktop cooler (Oxford Cryosystems). Data collection strategy and data reduction followed standard procedures implemented in the *CrysAlisPro* software (Oxford Diffraction, 2009). Differential scanning calorimetry (DSC) was carried out with a Shimadzu DSC-60 instrument (Shimadzu, Kyoto, Japan). Powdered samples weighing 2–4 mg were heated in open aluminium pans at a rate of 10 K min$^{-1}$ under a nitrogen gas flow of 30 ml min$^{-1}$. Raman spectra were recorded with a LabRAM HR Horiba Jobin Yvon Raman system equipped with two monochromator gratings and a charge-coupled device detector. A 1800 g mm$^{-1}$ grating and a 100 µm hole resulted in a spectral resolution of 1.5 cm$^{-1}$. The He–Ne laser line at 632.8 nm was used as an excitation source. Special care was taken to ensure minimal heating and no sample alteration. The spectra were acquired on powder samples at both sides of the phase transition, with temperatures controlled by Linkam Examina THMS600 Temperature Controlled Stage.

### 2.1. Synthesis and crystallization

*Iqtp* was prepared by using the one-pot method reported by Wang & Hanan (2005). The solvents were purchased from commercial sources and used without further purification, while 4-acetylpyridine and 4-isoquinolinecarboxaldehyde were obtained from Aldrich.

Synthesis: 4-Acetylpyridine (0.61 g 5.0 mmol) was added to a solution of 4-isoquinolinecarboxaldehyde (0.40 g, 2.5 mmol) in EtOH (20 ml) and the mixture was stirred for 0.25 h. KOH pellets (0.30 g, 5.4 mmol) with excess aqueous $NH_3$ (8.0 ml, 25%, 107 mmol) were added. The resulting solution was stirred at room temperature over a period of 5 h. The light-brown precipitate formed was filtered off and washed with water (4 × 10 ml). The product was dissolved in $CH_2Cl_2$ (15 ml), filtered and transferred to a 50 ml round-bottom flask



Files: b/eb5043/eb5043.3d b/eb5043/eb5043.sgml EB5043 FA IU-1517/5(16)11 1516/47(16)11 (100) EB5043 PROOFS B:FA:2015:71:6:0:0–0

**Table 1**
Experimental details for (I) and (II).

For all structures: $C_{24}H_{16}N_4$, $M_r$ = 360.41. Experiments were carried out with Mo $K\alpha$ radiation using an Oxford Diffraction Gemini CCD S Ultra diffractometer. Absorption was corrected for by multi-scan methods, *CrysAlisPro* (Oxford Diffraction, 2009). H-atom parameters were constrained.

| | (II) at 170 K | (II) at 220 K | (II) at 274 K | (I) at 277 K | (I) at 293 K |
|---|---|---|---|---|---|
| Crystal data | | | | | |
| Crystal system, space group | Monoclinic, $P2_1/n$ | Monoclinic, $P2_1/n$ | Monoclinic, $P2_1/n$ | Monoclinic, $P2_1/c$ | Monoclinic, $P2_1/c$ |
| $a$, $b$, $c$ (Å) | 23.9426 (4), 10.4477 (2), 14.9833 (2) | 24.0305 (5), 10.4656 (2), 15.0315 (4) | 24.2412 (2), 10.4907 (4), 15.0278 (9) | 12.2957 (2), 10.5239 (2), 14.9250 (3) | 12.3277 (3), 10.5211 (2), 14.9441 (4) |
| $\beta$ (°) | 106.145 (2) | 106.303 (3) | 106.656 (5), | 107.508 (2) | 107.638 (2) |
| $V$ (Å$^3$) | 3600.15 (10) | 3628.30 (15) | 3661.3 (3) | 1841.79 (7) | 18 47.15 (8) |
| $Z$ | 8 | 8 | 8 | 4 | 4 |
| Radiation type | Mo $K\alpha$ | Mo $K\alpha$ | Mo $K\alpha$ | Mo $K\alpha$ | Mo $K\alpha$ |
| $\mu$ (mm$^{-1}$) | 0.08 | 0.08 | 0.08 | 0.08 | 0.08 |
| Crystal size (mm) | 0.28 × 0.20 × 0.10 | 0.28 × 0.20 × 0.10 | 0.28 × 0.20 × 0.10 | 0.28 × 0.20 × 0.10 | 0.28 × 0.20 × 0.10 |
| Data collection | | | | | |
| No. of measured, independent and observed reflections | 58 228, 7341, 5379 | 43 182, 7397, 4918 | 28 207, 7461, 4247 | 36 886, 3773, 2653 | 36 721, 3785, 2672 |
| $R_{int}$ | 0.056 | 0.058 | 0.060 | 0.048 | 0.059 |
| $(\sin \theta/\lambda)_{max}$ (Å$^{-1}$) | 0.625 | 0.625 | 0.625 | 0.625 | 0.625 |
| Refinement | | | | | |
| $R[F^2 > 2\sigma(F^2)]$, $wR(F^2)$, $S$ | 0.044, 0.127, 1.09 | 0.049, 0.135, 1.01 | 0.062, 0.176, 1.10 | 0.046, 0.118, 1.02 | 0.048, 0.134, 1.04 |
| No. of reflections | 7341 | 7397 | 7461 | 3773 | 3785 |
| No. of parameters | 506 | 506 | 506 | 272 | 273 |
| No. of restraints | 0 | 0 | 0 | 18 | 19 |
| $\Delta\rho_{max}$, $\Delta\rho_{min}$ (e Å$^{-3}$) | 0.23, −0.20 | 0.18, −0.18 | 0.39, −0.21 | 0.14, −0.15 | 0.16, −0.14 |

Computer programs used: *CrysAlisPro* (Oxford Diffraction, 2009), *SHELXS* (Sheldrick, 2008), *SHELXL*2014/6 (Sheldrick, 2015), *PLATON* (Spek, 2009).

with a ground glass joint where the solvent was vacuum eliminated. Ethanol (5 ml) was added to the solid and the flask was closed. The mixture was heated in a water bath at 353 K with continuous shaking until the formation of the crystals, and then was allowed to stand undisturbed at room temperature for 0.5 h. The well formed colourless crystals were separated by filtration and washed with diethyl ether (3 × 5 ml) (yield: 0.30 g, 33%). ESI–MS (MeOH) $m/z$ 361.2 $[M+H]^+$ (calc. 361.4). Anal.: calc. for $C_{24}H_{16}N_4$: C 79.98, H 4.47, N 15.55; found: C 79.90, H 4.49, N 15.53%. ATR FT–IR (cm$^{-1}$): 3050(w), 3026(w), 2978(w), 1594(s), 1558(m), 1545(m), 1529(m), 1499(m), 1458(w), 1434(m), 1423(m), 1389(s), 1317(m), 1262(m), 1229(w), 1216(m), 1178(w), 1161(w), 1136(w), 1088(w), 1066(m), 1017(w), 993(m), 963(w), 904(m), 879(m), 828(s), 800(m), 789(s), 755(s), 671(m), 645(s), 626(s). $^1$H NMR (300 MHz, $CDCl_3$, 298 K) $\delta$/p.p.m.: 9.24 (s, 1H, $H^{C1}$), 8.47 (s, 1H, $H^{C3}$), 7.77 (m, 1H, $H^{C5}$), 7.65 (m, 1H, $H^{C6}$), 7.58 (m, 1H, $H^{C7}$), 8.00 (m, 1H, $H^{C8}$), 7.92 (s, 2H, $H^{B3,\ B5}$), 7.98 (d, 4H, $H^{A3,A5,D3,D5}$), 8.65 (d, 4H, $H^{A2,\ A6,\ D2,\ D6}$); $^{13}$C-PND and $^{13}$C-DEPT NMR (75 MHz, $CDCl_3$, 298 K) $\delta$/p.p.m.: 153.6 (CH, $C^{C1}$), 142.6 (CH, $C^{C3}$), 133.4 (Cquat, $C^{C4}$), 123.7 (CH, $C^{C5}$), 131.6 (CH, $C^{C6}$), 127.9 (CH, $C^{C7}$), 128.4 (CH, $C^{C8}$), 130.3 (Cquat, $C^{C9}$), 130.3 (Cquat, $C^{C10}$), 147.9 (Cquat, $C^{B4}$), 121.9 (2CH, $C^{B3,\ B5}$), 155.2 (2Cquat, $C^{B2,\ B6}$), 145.7 (2Cquat, $C^{A4,\ D4}$), 121.2 (4CH, $C^{A3,\ A5,\ D3,\ D5}$), 150.5 (4CH, $C^{A2,\ A6,\ D2,\ D6}$). The melting point was 538–540 K.

### 2.2. Refinement

The structures were solved using *SHELXS*97 (Sheldrick, 2008) and refined using full-matrix least squares with *SHELXL*2014 (Sheldrick, 2015). Form (I) presents one of the pyridine rings disordered into two well defined positions which were refined with restraints both in geometry as in anisotropic displacement factors (SAME and EADP instructions in *SHELXL*2014). The final occupation factors at 293 K converged to 0.468 (3) for fraction A and 0.532 (3) for fraction B. All H atoms were initially found in a difference map, and further idealized (with C-—H = 0.93 Å) and refined using a riding model, with isotropic $U_{iso}$(H) = 1.2*$U_{eq}$(C).

## 3. Results and discussion

### 3.1. Description of the structure(s)

X-ray diffraction data were collected at different temperatures, well above (293 K) and below the transformation (170 and 220 K), plus two experiments flanking the transition at 274 and 277 K ($T_c$, as seen by XRD, lays in the range 275–276 K).

The compound presents two different monoclinic structures at both sides of $T_c$, a high-temperature structure (I), crystallizing in $P2_1/c$ with almost no variations in the 277–293 K temperature range investigated, and a low-temperature counterpart (II), in $P2_1/n$, stable between 170 and 274 K. In this latter phase the structure preserves cell orientation but shows a doubling of the $a$ axis. (*Nota bene*: an heterodox

**Table 2**
Relevant torsion angles in (I) (293 K) and (II) (170 K).

| | (I) (293 K) (°) | | (II) (170 K) (°) | |
|---|---|---|---|---|
| | Disordered fraction *A* | Disordered fraction *B* | Moiety *A* | Moiety *B* |
| C4—C5—C6—C7 | 24.0 (7) | −11.2 (6) | 25.1 (2) | −11.5 (2) |
| C9—C10—C11—C12 | 7.8 (3) | | 12.3 (2) | 11.7 (2) |
| C9—C8—C16—C24 | 83.78 (18) | | 86.45 (17) | 87.09 (17) |

setting of $P2_1/n$ with $a > c$ was chosen in order to facilitate comparison with the $P2_1/c$ phase). Table 1 presents crystal data for both forms between 170 and 293 K.

In its high-temperature form (I) the compound presents one single molecule in the asymmetric unit with the disordered pyridine ring Cg1 split up into two well defined positions, Cg1*A* and Cg1*B* (in the following we shall refer to rings by their centroid codes, Fig. 1), while in form (II) this disorder in resolved into two ordered independent molecules, *A* and *B*.

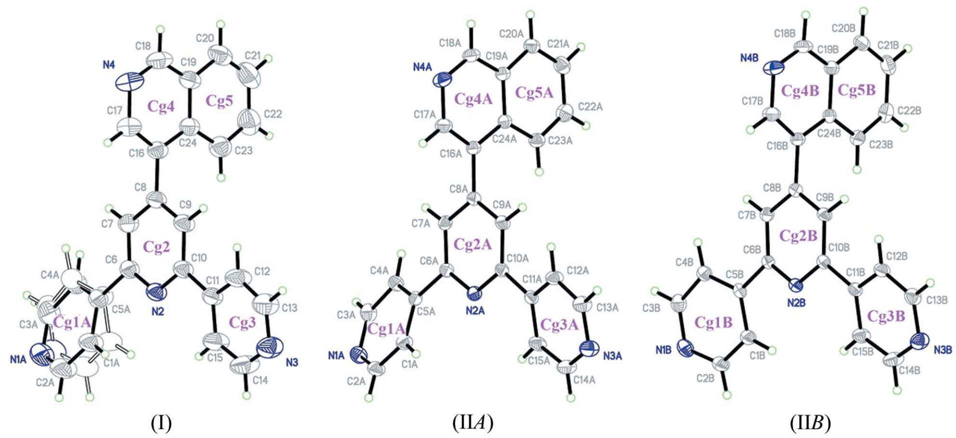


**Figure 1**
Molecular view of the unique molecule in (I) (293 K, with the disordered pyridine groups shown in different blackness; only the *A* fraction has been labelled) and the two independent molecules in (II) (170 K). Displacement ellipsoids drawn at the 40% level.

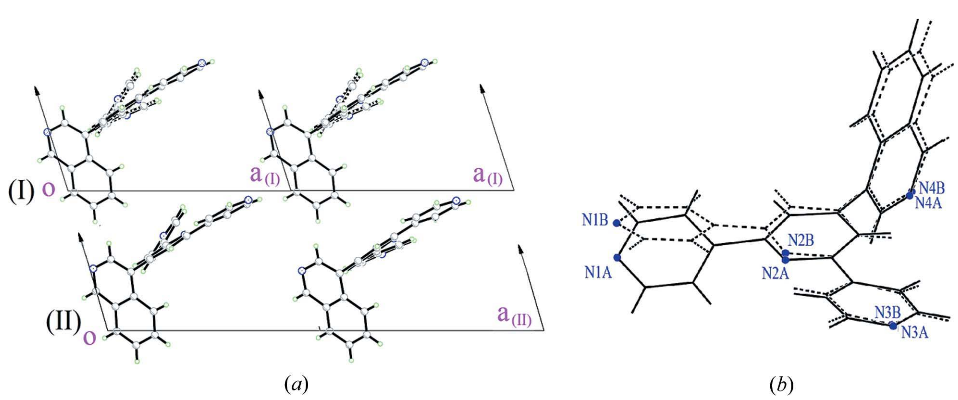


**Figure 2**
(*a*) Schematic projection of both monoclinic cells along "b", showing the way in which duplication of the "a" axis (**I→II**) takes pace. (*b*) Superposition of both independent molecules in (II), through a simple 1/2 $\boldsymbol{a}_{\mathbf{(II)}}$ translation (see text).

Fig. 1 presents a view of all three molecules [(I), at 293 K; (II*A*), (II*B*), at 170 K] with their numeration scheme. Fig. 2 (left) shows the way in which duplication along *a* takes place, while Fig. 2 (right) presents a view of the molecular 'misfit' between (II*A*)–(II*B*) molecules resulting from a pure $\frac{1}{2}$ $\mathbf{a}_{\mathbf{(II)}}$ translation (no further fitting/adjustment performed, save a rotation of the whole group in order to provide a clearer view). This should be compared with an eventual similar movement in (I) by a $\mathbf{a}_{\mathbf{(I)}} \simeq 1/2\ \mathbf{a}_{\mathbf{(II)}}$ translation, where both molecules [somehow a statistical 'average' of the two independent forms in (II)] would have a perfect overlap due to this movement corresponding to a genuine full cell translation.

The group:subgroup relationship between both structures is explained in detail in Fig. 3. The leftmost figures present two juxtaposed $P2_1/c$ cells, corresponding to form (I) (coloured backgrounds in the picture represent one single unit cell). The rightmost figure presents in turn the same basic scheme after deletion of a number of screw axis and inversion centres (crossed out in red) as well as the equivalent positions they give rise to (crossed out in blue) end up with the $P2_1/n$ space group representation corresponding to form (II).

As disclosed by Gavezzotti (2007), it is not uncommon to find crystals which undergo phase transitions where the structures differ in the doubling of one cell parameter, changing from one space group into a subgroup with lower symmetry. This situation, however, has not always been detected. For instance, in a first-order transformation reported by Ilczyszyn *et al.* (2008), the authors correctly report the space groups as $P2_1/c$ ($T$ = 200 K) and $P2_1/n$ ($T$ = 100 K), and comment on a cell doubling with 'significant increase of ***a*** and ***c*** lattice constants' (≃ 25% and 60%, respectively). However, a simple (***abc***) → (−***cba***) transformation applied to the $P2_1/n$ low-temperature structure leads to an almost perfect fit between the 200 K ($P2_1/c$) and the 100 K ($P2_1/n$) supramolecular arrangements, with ***c***:***c′*** and ***a***:***a′*/2** percentual differences of 0.6 and 0.2%, respectively and an identical relationship between

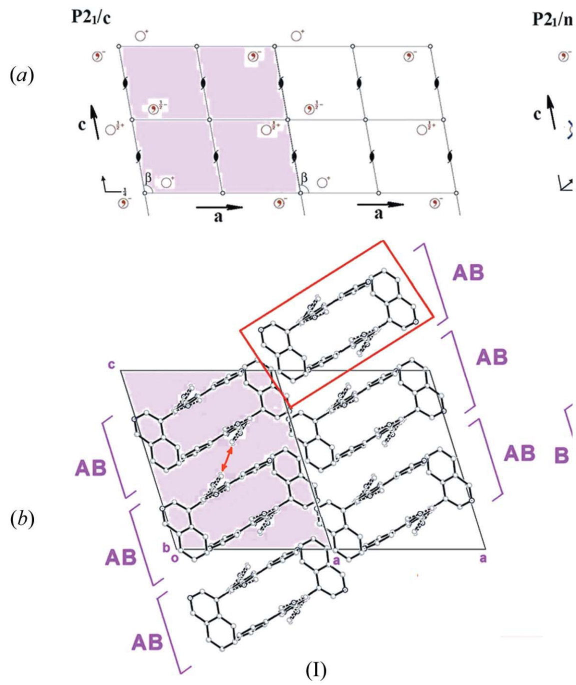


**Figure 3**
(*a*) Schematic representation of the group:subgroup relationship. (*b*) Comparison of slanted planar arrays formed in (I) and (II). Highlighted: the [010] columns seen in projection; H atoms not shown. The double arrow pinpoints the site where the eventual coexistence of forms *A* in (I) is forbidden, due to steric hindrance [H1*A*···H2*A*$(1-x, -y, 1-z)$: 1.90 Å].

symmetry elements as the one reported herein.

Regarding molecular structure, differences between (I), (II*A*) and (II*B*) are rather small, with little significance when bond distances and angles are compared (Tables S1 and S2 in the supporting information), but detectable in torsion angles of the three rotable bonds of each molecule: C5—C6, C10—C11, C8—C16. Table 2 presents a comparison of corresponding torsion angles, while Fig. 4 shows a comparative overlap of all three molecules where only the central ring Cg2 has been used for the least-squares fitting. Inspection of the figure and table confirms that differences reside in the relative ring orientations, with differences being rather smooth in Cg3 (mainly with a 'flapping' component) and in the fused Cg4—Cg5 system (with a minor component of rotation) but important in Cg1, with a dominating rotation effect around the C5—C6 bond.

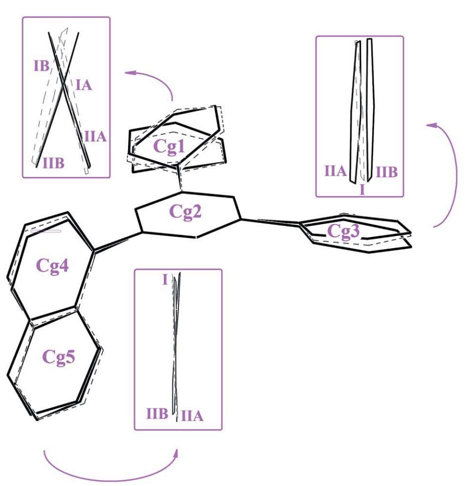


**Figure 4**
Comparison of the three independent molecules, through the least-squares fit of ring Cg2 only. In bold/broken lines: structure (II) (170 K, both molecules)/structure (I) (293 K). Inserts: detailed views of the sensitive regions, projected along the rotable bonds C5—C6, C10—C11, C8—C16.

### 3.2. Phase transition

The phase transition connecting both forms was consistently characterized by DSC, Raman spectroscopy and single-crystal XRD as first order, reversible, with a small hysteresis on heating–cooling and with no obvious damage to the structure upon cycling.

**3.2.1. DSC experiments**. DSC runs were made on powder samples, between 170 and 370 K with a heating/cooling rate of 10 K min$^{-1}$. The diagrams are basically featureless except in the 270–280 K region (Fig. 5) which shows an endothermic peak on heating, at 276 K, and an exothermal one on cooling at $T_{\rm cooling}$: 272 K. The onset temperatures, however, are quite similar (about 274 K). The $\Delta H$ involved was estimated to be *ca* 0.72 (6) kJ mol$^{-1}$ on heating/cooling.

**3.2.2. Raman experiments**. Extended Raman spectra of powder samples of the title compound were taken in the 293–170 K temperature range, within the 100 and 3500 cm$^{-1}$ region. In order to follow the phase transition in detail, further spectra were acquired on cooling the sample from room temperature to 213 K in steps of 2 K and then heating it back at the same rate. The phase transition, as detected by the vibrational properties, appears at 271–273 K on cooling and 275–277 K on heating, and appears in the form of splitting (at low temperature) of those peaks corresponding to intramolecular modes. A fact consistent with the presence of two independent molecules in the unit cell due to the breaking of the translational symmetry along ***a***, in contrast with the

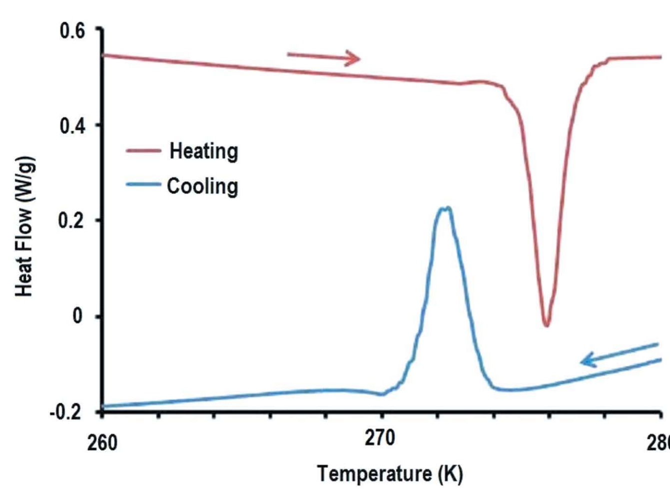


**Figure 5**
DSC runs, taken at 10 K min$^{-1}$.

presence of only one independent molecule at room temperature (Fig. 6).

It must be emphasized that even if the theoretical precision of the heating–cooling stage is 0.1 K, the true temperature of the sample could differ from the measured one due to heating under the laser beam (typically 3–4 K for transparent samples).

**3.2.3. Single-crystal XRD**. The evolution of the cell parameters with temperature, as measured by single-crystal XRD, clearly shows the first-order character of the (I) ↔ (II) transformation: the jumps at the transition temperature shown in Fig. 7, albeit small, are clear. Another characteristic differentiating first-order transformations from second-order ones is the coexistence of phases in the vicinity of $T_c$. Fig. 8 shows a series of X-ray diagrams taken at different temperatures, at fixed angles, with spots corresponding to form (II) being labelled in black and those of form (I) in red (time

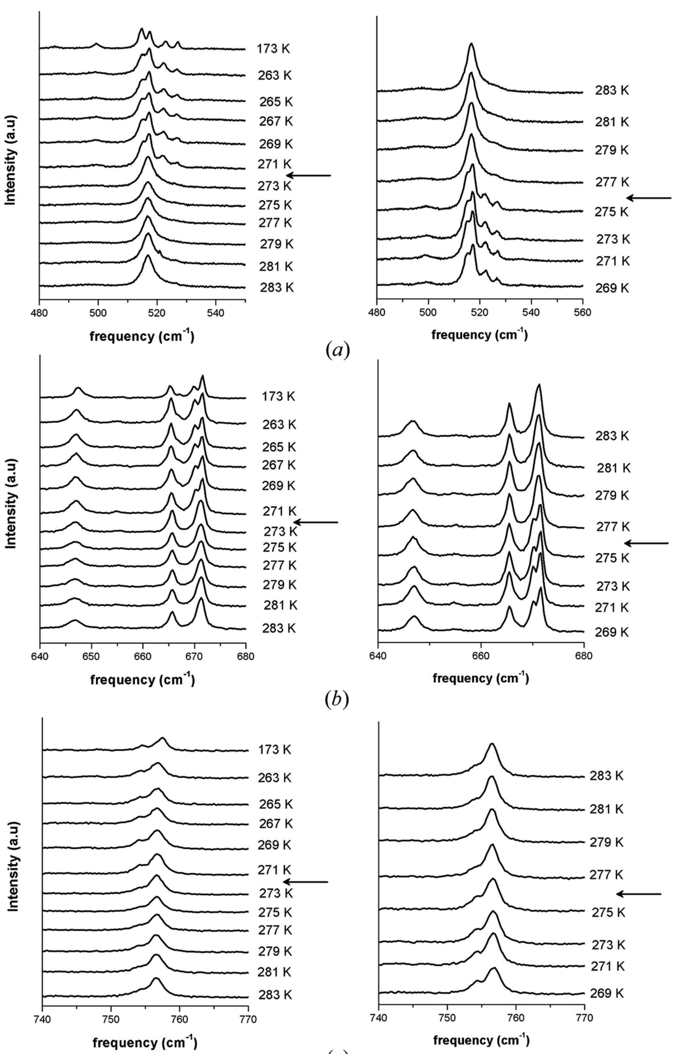


**Figure 6**
Selected peaks in the Raman spectra, showing the way in which line splitting discloses the phase transition. The left-hand column corresponds to sample cooling while the right-hand one corresponds to heating. Horizontal arrows show the transformation onsets. (*a*) 480–560 cm$^{-1}$; (*b*) 640–680 cm$^{-1}$; (*c*) 740–770 cm$^{-1}$.

**Table 3**
C—H···N and C—H···π interactions (Å, °) in (I) (293 K) and (II) (170 K).

| | *D*—H···*A* | *d*(*D*—H) | *d*(H···*A*) | *d*(*D*···*A*) | ⟨*D*—H···*A*⟩ |
|---|---|---|---|---|---|
| (I) | | | | | |
| #1I | C9—H9···N1$B^{i}$ | 0.93 | 2.59 | 3.520 (3) | 174 |
| #2I | C12—H12···N1$A^{i}$ | 0.93 | 2.57 | 3.498 (3) | 173 |
| #3I | C4*B*—H4*B*···N4$^{ii}$ | 0.93 | 2.50 | 3.309 (7) | 146 |
| #4I | C22—H22···Cg1$A^{iii}$ | 0.93 | 2.62 | 3.504 (4) | 171 |
| #5I | C22—H22···Cg1$B^{iii}$ | 0.93 | 3.00 | 3.913 (3) | 168 |
| (II) | | | | | |
| #1II | C9*B*—H9*B*···N1$B^{i}$ | 0.93 | 2.56 | 3.4665 (18) | 165 |
| #2II | C12*A*—H12*A*···N1$A^{i}$ | 0.93 | 2.57 | 3.495 (2) | 175 |
| #3II | C4*B*—H4*B*···N4$A^{iv}$ | 0.93 | 2.54 | 3.368 (2) | 149 |
| #4II | C22*A*—H22*A*···Cg1$B^{v}$ | 0.93 | 2.82 | 3.700 (2) | 157 |
| #5II | C22*B*—H22*B*···Cg1$A^{vi}$ | 0.93 | 2.62 | 3.538 (2) | 169 |
| #6II | C4*A*—H4*A*···Cg3$A^{iv}$ | 0.93 | 2.92 | 3.4251 (17) | 115 |
| #7II | C15*A*—H15*A*···Cg5$A^{iv}$ | 0.93 | 2.97 | 3.7204 (16) | 138 |
| #8II | C3*B*—H3*B*···Cg4$B^{vii}$ | 0.93 | 2.95 | 3.8289 (7) | 159 |
| #9II | C7*A*—H7*A*···N4$B^{iv}$ | 0.93 | 2.61 | 3.422 (2) | 146 |

Ring codes: as in Fig. 1. Symmetry codes: (i) $x, 1+y, z$; (ii) $-x, -\frac{1}{2}+y, \frac{1}{2}-z$; (iii) $x, \frac{1}{2}-y, -\frac{1}{2}+z$; (iv) $\frac{1}{2}-x, -\frac{1}{2}+y, \frac{1}{2}-z$; (v) $-\frac{1}{2}+x, \frac{1}{2}-y, -\frac{1}{2}+z$; (vi) $\frac{1}{2}+x, \frac{1}{2}-y, -\frac{1}{2}+z$; (vii) $x, -1+y, z$.

elapsed between frames: approximately 30 min). **Extrememost frames show only form (II) (*T*: 170 K) and form (I) (*T*: 293 K) phases, respectively**. Intermediate photographs taken in the transition region 274–277 K show instead the coexistence of phases with a gradual vanishing of the low-temperature $31\overline{4}$ reflection [forbidden in form (I) due to ***a*** axis doubling: $\mathbf{h}_{\mathbf{(II)}}$ = odd → $\mathbf{h}_{\mathbf{(I)}}$ = non-integer] and the gradual

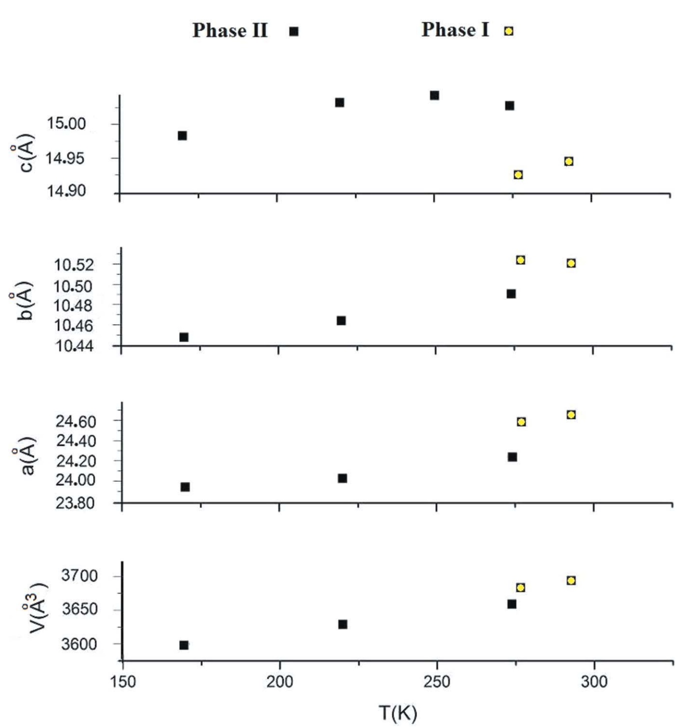


**Figure 7**
Evolution of cell parameters with temperature. Values for ***a*** and *V* in (I) have been duplicated to facilitate comparison with (II).

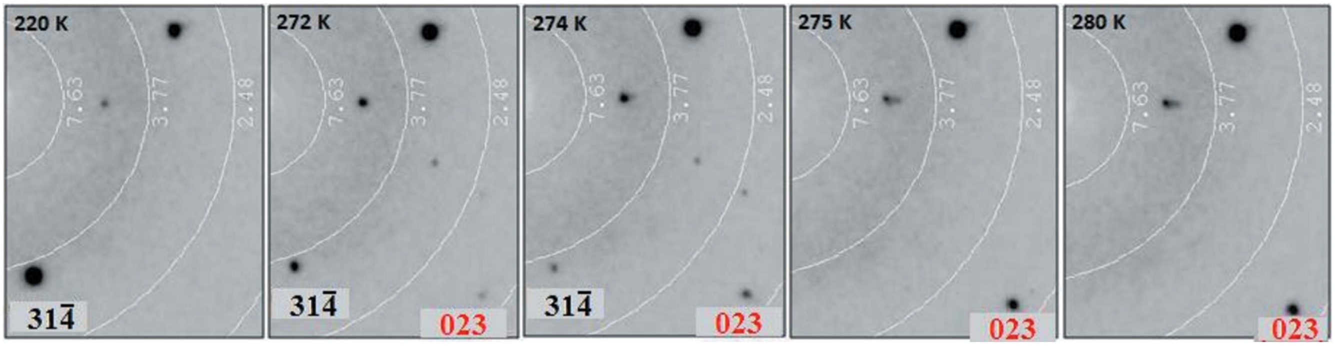


**Figure 8**
Sequence of single-crystal X-ray diffraction diagrams showing the evolution of phases with temperature (time elapsed between frames: approximately 30 min). Note the coexistence of phases in the vicinity of $T \simeq 275$ K: spot 31$\bar{4}$ corresponds to phase (II); spot 023, to phase (I).

**Table 4**
$\pi\cdots\pi$ interactions in (I) (293 K) and (II) (170 K).

CCD: center-to-center distance (distance between ring centroids); DA: dihedral angle (angle between ring planes); IPD: interplanar distance (mean distance from one plane to the neighbouring centroid); SA: slippage angle (mean angle subtended by the intercentroid vector to the plane normal).

| | Cg···Cg′ | CCD | DA | SA | IPD |
|---|---|---|---|---|---|
| (I) | | | | | |
| #6I | Cg1*B*···Cg3$^{i}$ | 3.7381 (19) | 7.9 (2) | 20 (3) | 3.50 (6) |
| #7I | Cg5···Cg5$^{ii}$ | 3.6766 (11) | 0 | 16.30 (1) | 3.529 (1) |
| #8I | Cg2···Cg3$^{iii}$ | 3.8428 (14) | 8.6 (2) | 20 (2) | 3.61 (7) |
| **II** | | | | | |
| #10II | Cg1*B*···Cg3*B*$^{iv}$ | 3.7204 (1) | 13 | 19 (6) | 3.50 (12) |
| #11II | Cg5*A*···Cg5*A*$^{ii}$ | 3.7856 (1) | 0 | 23.70 (2) | 3.464 (1) |
| #12II | Cg5*B*···Cg5*B*$^{iii}$ | 3.5343 (1) | 0 | 10.1 | 3.479 (1) |
| #13II | Cg2*A*···Cg3*B*$^{v}$ | 3.7717 (1) | 17 | 21 (7) | 3.50 (15) |
| #14II | Cg2*B*···Cg3*A*$^{v}$ | 3.8870 (1) | 9 | 21.8 (9) | 3.61 (3) |

† Ring codes: as in Fig. 1. Symmetry codes: (i) $1-x, -\frac{1}{2}+y, \frac{1}{2}-z$; (ii) $-x, 1-y, -z$; (iii) $1-x, 1-y, -z$; (iv) $\frac{3}{2}-x, -\frac{1}{2}+y, \frac{1}{2}-z$; (v) $1-x, 1-y, 1-z$.

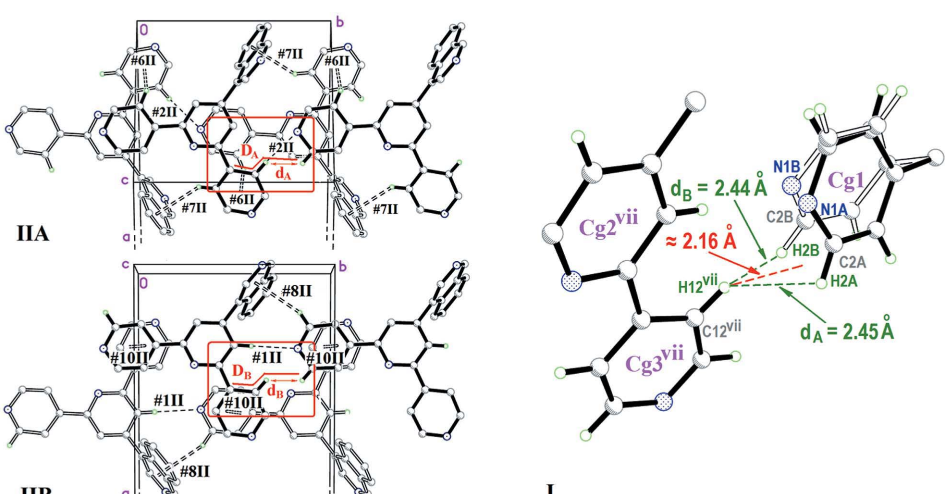


**Figure 9**
(*a*) Projection showing in detail the [010] columns in (II). (*b*) A detailed view of the way in which Cg1 rings in (I) split at both sides of the perturbing H12$^{vii}$ near neighbour. Only those H atoms taking part in the interactions are shown. Symmetry code: (vii) $x, -1+y, z$. Interaction codes as in Tables 2 and 3.

appearance of the high-temperature 023 reflection, absent in the previous diagrams.

### 3.3. Intermolecular interactions and the phase transition mechanism

Looking for eventual connections between intermolecular interactions and the phase transition we analyzed in detail differences and similarities in the supramolecular structures. The (rather weak) links responsible for the crystal packing in both phases are presented in Tables 3 (C—H···N, C—H···$\pi$) and 4 ($\pi\cdots\pi$). In the following these interactions will be addressed by the '#*n*' code appearing in the first column.

A first analogy between forms (I) and (II) are the helicoidal columns parallel to [010] which build up around the screw axis in both forms, which could be somehow considered as structural motives in the supramolecular organization. Even if the specific interactions involved in the formation of these columns are slightly different in each form, the general aspects are the same, *viz.* the symmetry operations involved in their generation are a ***b*** translation and a $\boldsymbol{2_1}$ rotation, both of them of the 'first kind' or 'enantiomer keeping', with molecules in each column being all of the same chirality. Furthermore, in form (II) they are built up by one single type of molecule (*A* or *B*), without mixing. Fig. 9 (left) shows the way in which this is achieved for columns (II*A*) and (II*B*), and views of these columns are shown in projection in Fig. 3(*b*). In structure (II), columns generated around the screw at $x$ = 1/4, $z$ = 1/4 involve only type *A* molecules, and the one at $x$ = 3/4, $z$ = 1/4 involve only type **B** molecules. From the effect of lateral inversion centres located in the [101] line, similar columns interact with each other and two different kinds of planar arrays (type $A$ or type $B$) parallel to $(10\overline{1})$ are generated. It is interesting to note that contacts in form (II) split into two different categories, *viz.* those linking similar molecules ($A$–$A$, $B$–$B$), interactions which are thus intraplanar, and those mixing them ($A$–$B$, $B$–$A$), which link neighbouring planes into a weakly bound three-dimensional structure. The alternation of type $A$ and type $B$ slabs is not present in (I), due to both types of molecules ($A$, $B$) being now essentially the same one. Due to cell metrics, the same plane orientation is now described as parallel to $(10\overline{2})$. Both dispositions are shown in Fig. 3(*b*).

Since the most significant differences between both forms reside in pyridyl rings Cg1 [disordered in (I), ordered in (II)], **it is reasonable to search the clues in this splitting for the phase transformation**. The highlighted regions in Fig. 9 (left) disclose a relevant difference between columns (II$A$) and (II$B$): while C12—H12$^{\rm vii}\cdots$H2 distances [(vii) $x, -1+y, z$] appear as non-interacting ($d_A$ = 2.45 Å, $d_B$ = 2.44 Å), this is achieved by the rotation of the pyridyl ring Cg1$A$/Cg1$B$ towards opposite sides with respect to the Cg3$^{\rm vii}$ plane, as disclosed by the sign of the dihedral angles $D_A$ = (C11—C12—H12)$^{\rm vii}$—H2$A$ = 152.7° and $D_{\rm B}$ = (C11—C12—H12)$^{\rm vii}$—H2$B$ = −133.4°. If trying to flip from one state to the other *via* a rotation around the C5—C6 bond, the system would go through a short (C12—H12)$^{\rm vii}\cdots$H2 distance of $\simeq$ 2.16 Å (Fig. 9, right). Even if small, at lower temperatures the barrier imposed by this hindrance could be high enough as to prevent flipping, and only when the temperature is raised enough (in our case to $T \simeq$ 272–274 K) the conversion into a disordered state would be possible. However, this process is not free of restraints and requires some partial order: neighbouring molecules in (I) linked by the symmetry operation (xii) $1-x, y, 1-z$ cannot have both the disordered pyridyl Cg1 in state $A$ because of a precluded bumping condition (H1$A\cdots$H2$A^{\rm xii} \simeq$ 1.90 Å; double arrow in Fig. 3*b*). In terms of occupations, this imposes the condition that the one for $A$ should be < 0.50, while there are no restrictions for $B$. This is in line with the results from the refinement [Oc($A$): 0.468 (3), Oc($B$) 0.532 (3)].

From the viewpoint of non-covalent interactions, Figs. 10 and 11 show the 'reversible switching' between contacts, occurring when going through the transition Cg1$A$ ↔ Cg1$B$: the C4$A$—H4$A\cdots$Cg3$A$ contact (#6II, Fig. 10*a*) switches to the Cg1$B\cdots$Cg3$B$ contact (#10II, Fig. 11*a*), mainly through the rotation of Cg1($A \rightarrow B$) with a dramatic change in the C4—C5—C6—C7 torsion angles (Table 2) by the resultant amount of 36.6 (4)°. Thus modifications in the type and strength of the prevailing interactions may play a relevant role in the transformation mechanism. In order to corroborate this fact these non-covalent interactions were analyzed using the Hirshfeld surface mapped with a shape index surface (*CrystalExplorer*; Wolff *et al.*, 2012), which represents regions where the molecular surfaces are in contact in a colored way (hollows represented in red, bumps in blue). In Fig. 10(*b*) the presence of a C—H$\cdots\pi$ contact is confirmed, with a typical large red colored concave curvature dominating the contact surface. By contrast, Fig. 11(*b*) shows a very different appearance of the same region, where now a pattern of red and blue triangles characteristic of $\pi\cdots\pi$ offset stacking, involving the Cg1$B$ and Cg3$B$ rings, dominates the contact surface.

The final issue remained as how to classify the present transition, *viz.* if it consists (or not) of a conformational transformation. The precedent discussion shows that no new conformers are generated, but an inter-conversion of pre-existent forms applies instead, in the form of an ordering–disordering process between them. The mild changes observed might even preclude the reference to phases (I) and (II) as 'polymorphs', and perhaps they should be better addressed as

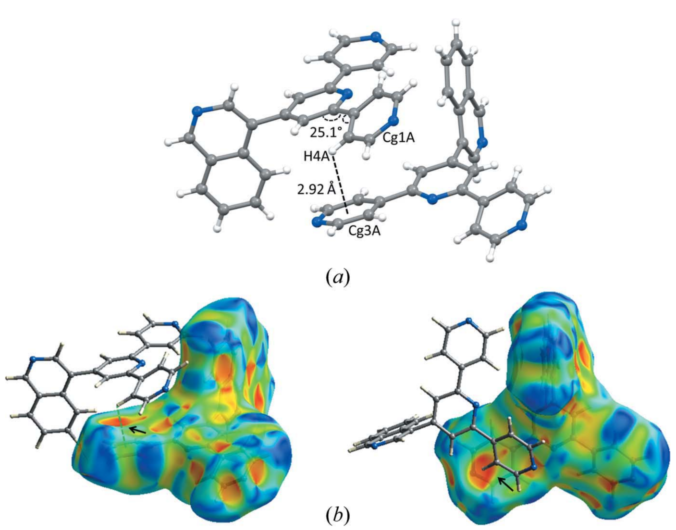


**Figure 10**
The #6II C—H$\cdots\pi$ intermolecular interaction in (II). (*a*) Molecular representation as generated by *Mercury* (Macrae *et al.*, 2008) and (*b*) two views of the Hirshfeld surface generated with *CrystalExplorer* (Wolff *et al.*, 2012), mapped with shape index. Small arrows pinpoint the red region.

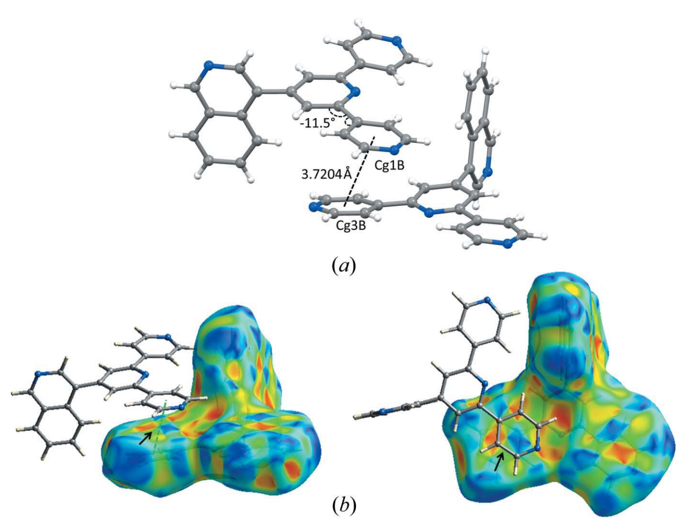


**Figure 11**
The #10II $\pi\cdots\pi$ intermolecular interaction in (II). (*a*) Molecular representation as generated by *Mercury* (Macrae *et al.*, 2008) and (*b*) two views of the Hirshfeld surface generated with *CrystalExplorer* (Wolff *et al.*, 2012), mapped with shape index. Small arrows pinpoint the red and blue triangles.

simple 'modifications', more in line with that discussed in Gavezzotti (2007).

## 4. Conclusion

The thermal behavior of *iqtp*, using single-crystal XRD, differential scanning calorimetry (DSC) and Raman scattering measurements was studied. The compound undergoes a reversible phase transition at 274 K, which appears to be first-order according to the coexistence of both phases in the vicinity of the transition and the observed abrupt jumps of the unit-cell parameters with temperature. On cooling, the transformation leads from a $P2_1/c$ symmetry ($z' = 1$) to $P2_1/n$ with duplication of the $a$ axis and the asymmetric unit content ($z' = 2$). The main structural differences observed at both sides of the transition are the splitting and slight rotations of some planar rings. This can be explained through the change of relevance of the weak interactions connecting them, something confirmed employing Hirshfeld surfaces.


## Acknowledgements

The authors acknowledge Universidad de La Frontera (Proyecto DIUFRO DI15-0027) and ANPCyT (project No. PME 2006-01113) for the purchase of the Oxford Gemini CCD diffractometer. The extremely helpful comments and suggestions received from the reviewers are gratefully acknowledged.


## References


Boldyreva, E. V., Arkhipov, S. G., Drebushchak, T. N., Drebushchak, V. A., Losev, E. A., Matvienko, A. A., Minkov, V. S., Rychkov, D. A., Seryotkin, Y. V., Stare, J. & Zakharov, B. A. (2015). *Chem. Eur. J.* **21**, doi: 10.1002/Chem.201501541.

Bučar, D.-K., Lancaster, R. W. & Bernstein, J. (2015). *Angew. Chem. Int. Ed.* **54**, 6972–6993.

Cave, G. W. V. & Raston, C. L. (2001). *J. Chem. Soc. Perkin Trans. 1*, pp. 3258–3264.

Constable, E. C., Housecroft, C. E., Kopecky, P., Neuburger, M., Zampese, J. A. & Zhang, G. (2012). *CrystEngComm*, **14**, 446–452.*a*

Constable, E. C., Housecroft, C. E., Neuburger, M., Schönle, J., Vujovic, S. & Zampese, J. A. (2013). *Polyhedron*, **60**, 120–129.*a*

Constable, E. C., Housecroft, C. E., Neuburger, M., Vujovic, S., Zampese, J. A. & Zhang, G. (2012). *CrystEngComm*, **14**, 3554–3563.*b*

Constable, E. C., Housecroft, C. E., Prescimone, A., Vujovic, S. & Zampese, J. A. (2014). *CrystEngComm*, **16**, 8691–8699.*a*

Constable, E. C., Housecroft, C. E., Schönle, J., Vujovic, S. & Zampese, J. A. (2013). *Polyhedron*, **62**, 260–267.*b*

Constable, E. C., Housecroft, C. E., Vujovic, S. & Zampese, J. A. (2014*a*). *CrystEngComm*, **16**, 328–338.*b*

Constable, E. C., Housecroft, C. E., Vujovic, S. & Zampese, J. A. (2014*b*). *CrystEngComm*, **16**, 3494–3497.*c*

Constable, E. C., Housecroft, C. E., Vujovic, S., Zampese, J. A., Crochet, A. & Batten, S. R. (2013). *CrystEngComm*, **15**, 10068–10078.*c*

Constable, E. C., Zhang, G., Housecroft, C. E., Neuburger, M. & Zampese, J. A. (2010). *CrystEngComm*, **12**, 3733–3739.

Constable, E. C., Zhang, G., Housecroft, C. E. & Zampese, J. A. (2011). *CrystEngComm*, **13**, 6864–6870.

Constable, E. C., Zhang, G., Housecroft, C. E. & Zampese, J. A. (2012*c*). *Inorg. Chem. Commun.* **15**, 113–116.

Cruz-Cabeza, A. J. & Bernstein, J. (2014). *Chem. Rev.* **114**, 2170–2191.

Drebushchak, T. N., Drebushchak, V. A. & Boldyreva, E. V. (2011). *Acta Cryst.* B**67**, 163–176.

Gavezzotti, A. (2007). *J. Pharm. Sci.* **96**, 2232–2241.

Heine, J., Schmedt auf der Günne, J. & Dehnen, S. (2011). *J. Am. Chem. Soc.* **133**, 10018–10021.

Hou, L. & Li, D. (2005). *Inorg. Chem. Commun.* **8**, 190–193.

Housecroft, C. E. (2014). *Dalton Trans.* **43**, 6594–6604.

Ilczyszyn, M., Chwaleba, D., Ciunik, Z. & Ilczyszyn, M. M. (2008). *Chem. Phys.* **352**, 57–64.

Klein, Y. M., Constable, E. C., Housecroft, C. E., Zampese, J. A. & Crochet, A. (2014). *CrystEngComm*, **16**, 9915–9929.*a*

Klein, Y. M., Constable, E. C., Housecroft, C. E. & Zampese, J. A. (2014). *Polyhedron*, **81**, 98–104.*b*

Kubicki, M. (2004). *Acta Cryst.* B**60**, 333–342.

Macrae, C. F., Bruno, I. J., Chisholm, J. A., Edgington, P. R., McCabe, P., Pidcock, E., Rodriguez-Monge, L., Taylor, R., van de Streek, J. & Wood, P. A. (2008). *J. Appl. Cryst.* **41**, 466–470.

Oxford Diffraction (2009). *CrysAlisPro.* Oxford Diffraction Ltd, Yarnton, Oxfordshire, England.

Pal, R., Reddy, M. B. M., Dinesh, B., Balaram, P. & Guru Row, T. N. (2014). *J. Phys. Chem. A*, **118**, 9568–9574.

Sheldrick, G. M. (2008). *Acta Cryst.* A**64**, 112–122.

Sheldrick, G. M. (2015). *Acta Cryst.* C**71**, 3–8.

Singh, U. P., Narang, S., Pachfule, P. & Banerjee, R. (2014). *CrystEngComm*, **16**, 5012–5020.

Spek, A. L. (2009). *Acta Cryst.* D**65**, 148–155.

Wang, J. & Hanan, G. R. (2005). *Synlett*, pp. 1251–1254.

Wolff, S. K., Grimwood, D. J., McKinnon, J. J., Turner, M. J., Jayatilaka, D. & Spackman, M. A. (2012). *CrystalExplorer*, Version 3.0. University of Western Australia.

Yoshida, J., Nishikiori, S.-I. & Kuroda, R. (2007). *Chem. Lett.* **36**, 678–679.

Acta Crystallographica Section B
**Structural Science, Crystal Engineering and Materials**
ISSN 2052-5206

# ORDER FORM

YOU WILL AUTOMATICALLY BE SENT DETAILS OF HOW TO DOWNLOAD AN ELECTRONIC REPRINT OF YOUR PAPER, FREE OF CHARGE. PRINTED REPRINTS MAY BE PURCHASED USING THIS FORM.

Please scan your order and send to jb@iucr.org

**INTERNATIONAL UNION OF CRYSTALLOGRAPHY**
5 Abbey Square
Chester CH1 2HU, England.

VAT No. GB 161 9034 76

Article No.: B151937-EB5043

| | |
|---|---|
| Title of article | A temperature-induced order–disorder phase transition in a novel 4-substituted 4,2:6′,4′′-terpyridine |
| Name | Ricardo Baggio |
| Address | Gerencia de Investigación y Aplicaciones, Centro Atómico Constituyentes, Comisión Nacional de Energía Atómica, Buenos Aires, Argentina |
| E-mail address (for electronic reprints) | baggio@cnea.gov.ar |

## OPEN ACCESS

IUCr journals offer authors the chance to make their articles open access on **Crystallography Journals Online**. For full details of our open-access policy, see http://journals.iucr.org/services/openaccess.html. For authors in European Union countries, VAT will be added to the open-access charge.

☐ I wish to make my article open access. The charge for making an article open access is **1000 United States dollars**.

## DIGITAL PRINTED REPRINTS

I wish to order . . . . . . . paid reprints

**These reprints will be sent to the address given above. If the above address or e-mail address is not correct, please indicate an alternative:**

## PAYMENT

Charge for open access **1000** USD Charge for reprints . . . . . . . . USD Total charge . . . . . . . USD

☐ A cheque for . . . . . . . USD payable to **INTERNATIONAL UNION OF CRYSTALLOGRAPHY** is enclosed

☐ I have an open-access voucher to the value of . . . . . . . USD Voucher No.

☐ An official purchase order made out to **INTERNATIONAL UNION OF CRYSTALLOGRAPHY** ☐ is enclosed ☐ will follow

Purchase order No.

☐ Please invoice me

☐ I wish to pay by credit card

*EU authors only*: VAT No:

| | |
|---|---|
| Date | Signature |

## OPEN ACCESS

The charge for making an article open access is **1000 United States dollars**. For authors in European Union countries, VAT will be added to the open-access charge.

A paper may be made open access at any time after the proof stage on receipt of the appropriate payment. This includes all back articles on **Crystallography Journals Online**. For further details, please contact support@iucr.org. Likewise, organizations wishing to sponsor open-access publication of a series of articles or complete journal issues should contact support@iucr.org.

## DIGITAL PRINTED REPRINTS

An electronic reprint is supplied free of charge.

Printed reprints without limit of number may be purchased at the prices given in the table below. The requirements of all joint authors, if any, and of their laboratories should be included in a single order, specifically ordered on the form overleaf. All orders for reprints must be submitted promptly.

Prices for reprints are given below in **United States dollars** and include postage.

| | Size of paper (in printed pages) | | | | |
|---|---|---|---|---|---|
| Number of reprints required | 1–2 | 3–4 | 5–8 | 9–16 | Additional 8's |
| 50 | 184 | 268 | 372 | 560 | 246 |
| 100 | 278 | 402 | 556 | 842 | 370 |
| 150 | 368 | 534 | 740 | 1122 | 490 |
| 200 | 456 | 664 | 920 | 1400 | 610 |
| Additional 50's | 86 | 128 | 178 | 276 | 116 |

## PAYMENT AND ORDERING

Cheques should be in **United States dollars** payable to **INTERNATIONAL UNION OF CRYSTALLOGRAPHY**. Official purchase orders should be made out to **INTERNATIONAL UNION OF CRYSTALLOGRAPHY**.

Orders should be returned by email to jb@iucr.org

## ENQUIRIES

Enquiries concerning reprints should be sent to support@iucr.org.